Catalysis Today 137 (2008) 350–356

Contents lists available at ScienceDirect

Catalysis Today

journal homepage: www.elsevier.com/locate/cattod

Photocatalytic oxidation of toluene in the gas phase: Modelling an annular photocatalytic reactor

Vesna Tomašić *, Franjo Jović, Zoran Gomzi

Faculty of Chemical Engineering and Technology, Department of Reaction Engineering and Catalysis, Savska Cesta 16, 10000 Zagreb, Croatia

ARTICLE INFO

Article history:
Available online 2 July 2008

Keywords:
Annular photocatalytic reactor
Toluene oxidation
TiO_2
Reactor modelling

ABSTRACT

Photocatalytic oxidation of toluene in the gas phase over UV-illuminated thin layer of titanium dioxide was studied. The reaction was performed in the annular photocatalytic reactor at the room temperature and at various space times. The inlet reacting mixture consisted of air containing toluene and water vapors. Dependence of the reaction rate on various operating variables (water content, inlet toluene concentration and gas flow rate) was examined. The catalytic activity for toluene removal was evaluated by measuring the inlet and outlet toluene concentrations with GC/FID at the steady-state conditions. The additional XRD and FTIR measurements were carried out to get better understanding of the catalytic properties.

Modelling analysis was carried out to investigate effect of the key parameters on the reactor performance. To understand complex interaction between the chemical reaction and mass transfer phenomena, experimental data were analysed and compared with three different mathematical models (one-dimensional (1D) model and two-dimensional (2D) models based on ideal flow and laminar flow conditions). The proposed models were verified by comparing the computer simulation data with the experimental laboratory results. It was found out that behaviour of the annular photocatalytic reactor was mainly limited by the interphase mass transfer. Finally, the 2D heterogeneous model, based on the assumed laminar flow through the reactor, appeared to be the most suitable model for a detailed description of the annular photocatalytic reactor used for air pollution remediation.

1. Introduction

Volatile organic compounds (VOCs) represent the important class of pollutants, usually found in the atmosphere of all urban and industrial areas. Photochemical oxidation, PCO (also referred to as the advanced oxidation processes, AOP) has become increasingly popular as an alternative to VOC removal purposes [1]. The first PCO was reported by Fujishima and Honda [2] who used a photoelectrochemical cell for water splitting and rutile TiO_2 as a (photo)catalyst. TiO_2-mediated heterogeneous photocatalysis for oxidation of VOC compounds at low concentrations has been extensively studied [3–5]. While most relevant studies have dealt with photodegradation in the liquid phase, degradation of gaseous organic compounds has gained importance only recently, predominantly for air purification [3–5]. A great variety of organic compounds can be oxidized by TiO_2 photocatalysis in the presence of molecular oxygen and/or water [6,7]. Most attention is given to ethylene [8], isopropanol [9], butane [9], heptane [10], acetone [11], methanol [11], 1-butanol [12], benzene [13], toluene [9,11,14,15], acetaldehyde [16], butyl acetate [17], dimethylformamide (DMF) [18], 1-butylamine [12], trichloroethylene (TCE) [9,11,19], chloroform [19], dichloromethane [19], carbon tetrachloride [19], and dichloroacetic acid [20].

In the last decade the mechanism of heterogeneous photocatalysis has been investigated by many researchers [7,12,21]. Deactivation of photocatalysts was found to be a crucial disadvantage of this technique in practice, especially for the oxidation of aromatics [10,22]. The oxygen-bearing compounds, especially benzoic acid, can cause irreversible loss in the photoactivity of TiO_2 catalysts [22]. According to the literature this can be retarded using binary catalyst, such as titania–silica [16,22], titania–vanadia [14,15], titania–iron [23], titania–tungsten [15,17] or titania–tin mixed oxide [19].

Recently, investigation of optimal reactor configurations has become an important research area in the field of PCO. Different laboratory reactor designs are reported in the literature, e.g. fixed bed annular reactor [6,9,17], batch reactor [11], semi-batch reactor with quartz flat window [19], circulating fluidized bed (CFB)

* Corresponding author. Tel.: +385 1 4597 281; fax: +385 1 4597 260.
E-mail address: vtomas@fkit.hr (V. Tomašić).

0920-5861/$ – see front matter © 2008 Elsevier B.V. All rights reserved.
doi:10.1016/j.cattod.2008.05.017

a	geometric surface area (m^2)
A_R	surface area of reactor (annulus) cross-section (m^2)
C_A	toluene concentration (g dm^{-3})
D_A	molecular diffusion coefficient of toluene in air (1 bar, 20 °C) (cm^2 s^{-1})
D_g	molecular diffusion coefficient (m^2 h^{-1})
k	reaction rate constant (kg m^{-3} min^{-1})
k_A	reaction rate constant (min^{-1} (Eq. (6)))
k_g	interphase mass transfer coefficient (m h^{-1})
K_a	adsorption equilibrium constant (kg^{-1} m^3)
L	length of reactor (m)
p	pressure (Pa)
$p(H_2O)$	partial pressure of water vapor in the gas mixture (Pa)
r	radial reactor coordinate (m)
r_A	reaction rate (mol h^{-1} kg^{-1})
R	diameter of reactor annulus (m)
RH	relative humidity
R/L	dimensionless geometric number
T	temperature (K)
u	fluid linear velocity (m h^{-1})
v_0	volume flow rate (m^3 h^{-1})
V	reactor volume (m^3)
X_A	toluene conversion
z	axial reactor coordinate (m)

Greek letters

η	dynamic viscosity (m^2 s^{-1})
θ	coverage of TiO_2 surface with toluene
Θ	Bragg angle (°)
κ	ratio of inner and outer reactor diameter
μ	kinematic viscosity (kg m^{-1} s^{-2})
ρ	density (kg m^{-3})
τ	space time (min)

Dimensionless parameters

Re	Reynolds number (modification for annular reactor), $Re = (2R(1-\kappa)u_m\rho)/\eta$
Sc	Schmidt number, $Sc = D_g\rho/\mu$
Sh	Sherwood number, $Sh = 0.705[Re(d/L)]^{0.43}Sc^{0.56}$

Subscripts

g	in the bulk gas phase
m	mean value
s	on the catalytic surface
u	inner
0	inlet

Superscript

*	saturation

reactor [24], microchannel reactor [14], honeycomb monolith reactor [25], TiO_2-coated fibre-optic cable reactor [26], annular venturi reactor (photo-CREC–air) [27], etc. However, further work is necessary to accurately model the PCO reactors and to find a kinetic model which gives a reliable description of experimental results.

In this work photocatalytic degradation of toluene, used as a model VOC, was performed with the catalytic TiO_2 layer coated on the annular reactor walls. The rate of toluene removal was investigated at different reaction conditions. The appropriate kinetic model was proposed. Finally, in order to describe behaviour of the annular PCO reactor different mathematical models have been developed and the results discussed.

2. Experimental

2.1. Catalysts preparation and characterization

The commercial TiO_2 powder catalyst was supplied by *Degussa* (*Aeroxide* P-25). Average diameter of the catalyst particles was 30 nm. Crystal structure was primarily based on anatase (70% anatase and 30% rutile). The surface area was 50 m^2 g^{-1} (BET). The TiO_2 layer was coated on the internal glass surface of the outer tube of the annular reactor. TiO_2 isopropanol slurry was used for this purpose. Homogeneous suspension (1 g TiO_2/100 ml isopropanol) was prepared using the ultrasound bath (to break particle agglomerations) and homogenizer. The suspension was poured into a rotating tube and simultaneously dried in the hot air. Coating was repeated several times to a desired thickness of the catalytic layer. The TiO_2-coated tube was heated at 110 °C for 2 h. TiO_2 loading density was 22.3 μg cm^{-2}. The catalyst was characterized by X-ray powder diffraction (XRD) and Fourier transform infrared (FTIR) spectroscopy. XRD experiments were carried out on a *Philips*® PW1730. The Cu Kα radiation was performed at 40 kV and the 30 mA current. Sample scans were collected between 3° and 75° (step 0.02°, integration time 2 s). FTIR spectroscopy experiments were performed on a *PerkinElmer*® Spectrum One FTIR spectrometer. Sample scans were collected between 4000 and 450 cm^{-1} with step 4 cm^{-1}.

2.2. Experimental apparatus and procedures

High purity synthetic air (20.5% O_2 in N_2, *Messer*) was gas carrier. Ultra-pure water and maximum purity grade toluene (*Aldrich*) were used to prepare the reaction mixtures. The appropriate concentration of toluene and water was obtained by vaporization of organic compound and water at the specified airflow rate and regulation with the mass flow controllers (*Cole Palmer*). The temperature of liquid-containing saturators was maintained at 20 °C. Then the secondary airflow was introduced into the mainstream to obtain desired concentration of the reactants. Relative humidity, RH, was varied from 0.06 to 0.61. Inlet toluene concentrations were in the range from 1.0 to 9.9 × 10^{-3} g dm^{-3}. Total flow rate of the reaction mixture was varied from 2.4 to 24.6 dm^3 h^{-1}. The airflow rate was set and the reaction mixture was passed through the dark photoreactor (without UV light) to reach the adsorption equilibrium. Then the UV light was turned on. Toluene concentrations were measured using gas chromatography and a FID detector. Conversion, X_A, was calculated with respect to toluene concentration. Space-time in the reactor was varied by changing total flow rate at the constant reactor volume.

2.3. Design of the annular photocatalytic reactor

The annular photoreactor was constructed using a Pyrex glass tube. The reactor was 265 mm long. The outer tube diameter was 53.8 mm, and the inner tube diameter was 23.8 mm. Total volume of the reactor, V, was 0.485 dm^3. Illumination of the reactor was provided by an 8 W fluorescent black light blue lamp which efficiently emitted UVA light at 315–400 nm, with a maximum wavelength at 352 nm and 368 nm (*Sylvania*®). The UV lamp was

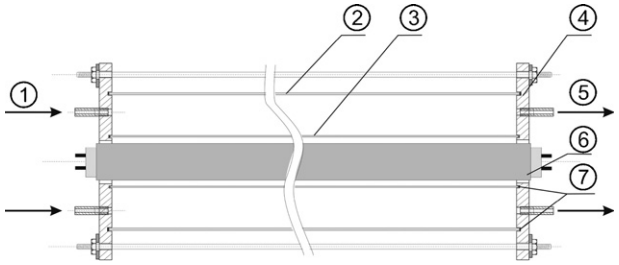

Fig. 1. Scheme of the photocatalytic annular reactor: (1) gas inlet, (2) outer tube with the catalyst layer, (3) inner tube, (4) end plate, (5) gas outlet, (6) UV tube and (7) rubber O ring.

in the central part of the reactor and protected by the inner tube of the annular reactor. The reaction gas mixture flew between the reactor's inner and outer tube (Fig. 1).

3. Results and discussion

3.1. The influence of water content on toluene conversion

According to the literature [28], water may have important role in the overall mechanism of photocatalytic reaction, serving as a source of hydroxyl radicals. The influence of water content on the rate of VOC photo-oxidation was investigated by many researchers, but different results were reported. Published data show that the surface of the TiO_2 catalysts is strongly hydrophilic and that preferential adsorption of water on the catalyst surface is responsible for low oxidation rate at high humidity [29]. However, our results pointed to a different trend. Higher relative humidity seems to retard formation of benzoic acid. This is of great practical importance because surface accumulation of benzoic acid appears to be responsible for catalytic deactivation. Fig. 2a shows the influence of relative humidity on toluene conversion under experimental conditions employed in this study. Water vapor content is calculated as relative humidity, RH, according to the following equation:

$$\mathrm{RH} = \frac{p(\mathrm{H_2O})}{p^*(\mathrm{H_2O})} \quad (1)$$

Saturation pressure of water vapor at the temperature of a gas mixture was calculated using Antoine equation [30]. According to the results from Fig 2a, relative humidity of the contaminated gas stream has small effect on toluene removal. With the increase of relative humidity from 0.061 to 0.610 at a constant flow rate and inlet toluene concentration toluene conversion increases from 0.044 to 0.132. These results show a different trend from that reported in the previous study [29].

3.2. Influence of the inlet toluene concentration

Fig. 2b shows influence of the inlet toluene concentration on toluene conversion at different flow rates of a gas mixture. As can be seen, conversion of toluene decreases with increased inlet toluene concentration in the whole range of the total flow rate. This can be attributed to a limited number of active sites on TiO_2 surface available for toluene adsorption. Therefore, by increasing the inlet toluene concentration a reactant passes through the reactor as unreacted.

3.3. Catalyst activity and stability

Over a prolonged period (after several days) toluene very slowly degrades, probably due to the catalyst deactivation. At the same time its colour gradually changes from white to light-yellow. Comparison between the XRD measurements for fresh and deactivated catalysts shows the absence of structural changes in the crystal lattice of TiO_2-deactivated catalyst (Fig. 3a). Yellow coloration may be the consequence of a by-product adsorption on the catalyst surface. Some authors confirmed that benzaldehyde and benzoic acid are responsible for deactivation of the TiO_2-based catalysts [10,22,29]. In our study, FTIR experiments (Fig. 3b) also confirmed the presence of benzaldehyde and benzoic acid on the surface of the TiO_2 catalysts. As can be seen, spectrum for the fresh catalyst reveals a relatively clean surface of the fresh TiO_2 catalyst. The band at 1623 cm^{-1} is assigned to the –OH band. Surface changes on a deactivated TiO_2 sample are indicated in the spectrum b) (Fig. 3b) where new bands appear at 1463, 1408, and 1285 cm^{-1}. The band at 1285 cm^{-1} is assigned to a weak absorption of aromatic aldehyde. The two bands at 1408 and 1463 cm^{-1} are results of interaction between the C–O and O–H of carboxylic acid. A detailed assignment of major IR bands is referred to in the literature [29]. Obviously, benzoic acid and benzaldehyde occur on the surface of the deactivated catalysts. Thus, the FTIR experiments confirm that deactivation of this type of catalyst arises from irreversible adsorption of the reaction intermediates, such as benzaldehyde and benzoic acid.

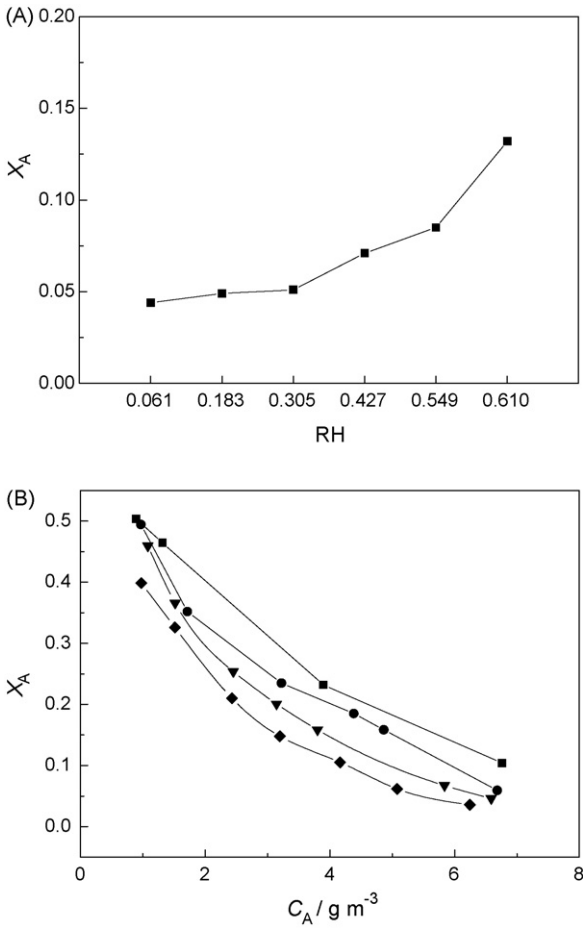

Fig. 2. Influence of relative humidity on conversion of toluene (reaction conditions: inlet toluene concentration = 9.9×10^{-3} g dm^{-3}; volume flow rate = 9.8 dm^3 h^{-1}) (A). Influence of the inlet toluene concentration on toluene conversion at different flow rates of a gas mixture (reaction conditions: volume flow rate = (■) 4.5; (●) 8.1; (▼) 12.3; (◆) 16.5 dm^3 h^{-1}; relative humidity = 0.25) (B).

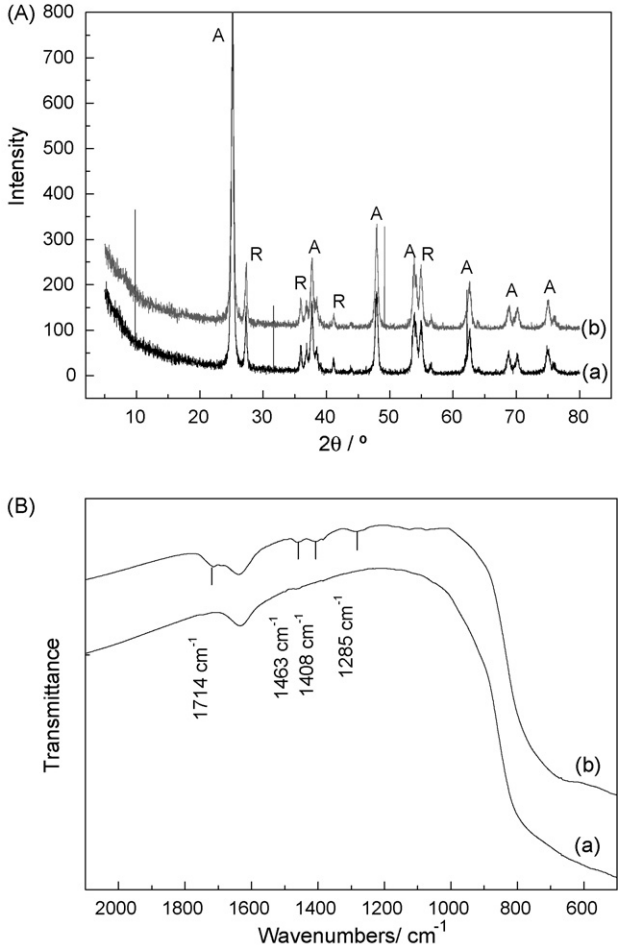

Fig. 3. XRD patterns of the catalysts for anatase (A) and rutile (R): (a) fresh TiO_2 and (b) deactivated TiO_2 (A). FTIR spectra: (a) fresh TiO_2 and (b) deactivated TiO_2 (B).

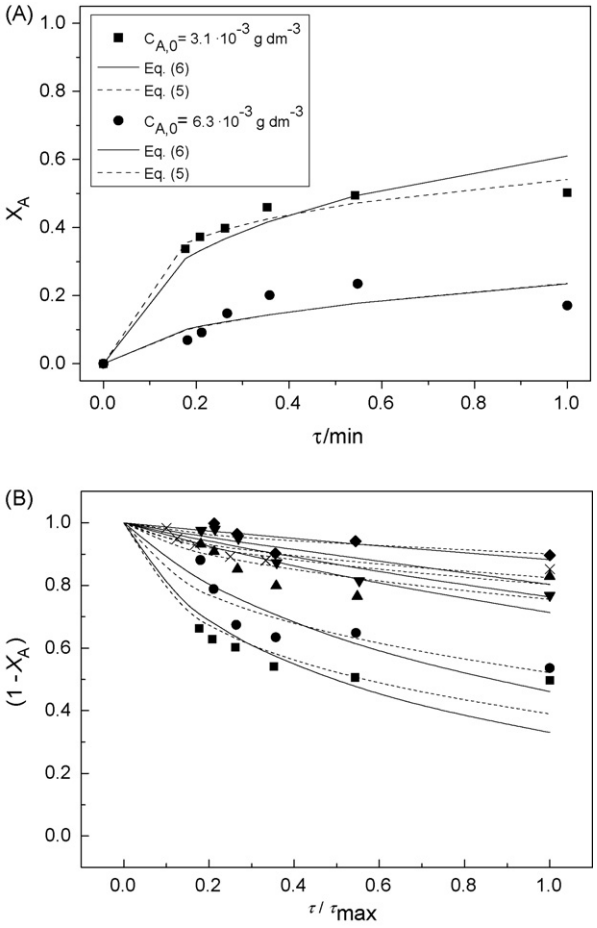

Fig. 4. Influence of the reactor space-time on toluene conversion: experimental data (points), the values predicted by Model I using Eq. (5) (dashed lines) and Eq. (6) (solid lines) (reaction conditions: inlet toluene concentration: (■) 3.1×10^{-3}; (●) 6.3×10^{-3} g dm^{-3}; relative humidity = 0.244) (A). Dimensionless toluene fractions versus normalized space-time at various inlet toluene concentrations: (■) 0.96×10^{-3}; (●) 1.55×10^{-3}; (▲) 3.14×10^{-3}; (▼) 4.06×10^{-3}; (◆) 6.30×10^{-3}; (×) 8.17×10^{-3} g dm^{-3} (Model I – solid lines and Model II – dashed lines) (B).

3.4. Effect of the total flow rate

The effect of space-time on toluene conversion at different inlet toluene concentrations at the entry to the reactor is shown in Fig. 4a. As expected, conversion of toluene increases by increasing space-time in the reactor (or by decreasing volume flow rate through the reactor). Obviously, a very long space-time leads to final equilibrium conversion.

3.5. The kinetics of toluene photooxidation

Generally, according to the Eq. (2) photooxidation of toluene results from interaction between the adsorbed toluene molecules and a hydroxyl radical. Adsorption of toluene (Eqs. (3) and (4)) is competitive with water adsorption. According to the previous conclusion about small influence of water content, toluene adsorption is probably the rate-determining step for this reaction:

$$C_7H^+_{8,ad} + HO^*_{ad} \rightarrow \text{products}(CO_2 + H_2O) \quad (2)$$

$$TiO_2(h^+) + C_7H_8 \rightarrow C_7H_{8,ad} \quad (3)$$

$$TiO_2(h^+) + C_7H_{8,ad} \rightarrow C_7H^+_{8,ad} \quad (4)$$

However, toluene photoxidation in the gas phase may result from a complex reaction mechanism, comprising numerous reactions [14]. Different by-products such as benzyl alcohol, benzaldehyde, benzoic acid and maleic anhydride can be formed by this complex reaction mechanism. As mentioned in the experimental part, the measure of the reaction extent in this study was an overall conversion of toluene. Therefore, in our kinetic analysis we used some simplifications. At constant oxygen and water vapor concentrations, considering that the reaction intermediates and products are weakly or non-competitively adsorbed, the Langmuir–Hinshelwood (LH) mechanistic kinetic model can be used to describe toluene degradation kinetics [31]:

$$r_A = \frac{kK_aC_A}{1 + K_aC_A} \quad (5)$$

Assuming that adsorption of toluene is a rate determining step ($K_a << 1$), the denominator in Eq. (5) equals 1, and the kinetic model can be reduced to the pseudo-first order reaction rate:

$$r_A = k_AC_A \quad (6)$$

3.6. Modelling the annular photocatalytic reactor

3.6.1. Assumptions and model equations

In essence, the approach to modelling an annular tubular photocatalytic reactor is similar to modelling other similar reactor configurations, e.g. a monolithic reactor. The main approach to our attempt is characterized by (a) the reactor is considered as stationary tubular reactor, i.e. inlet and outlet characteristic variables are time-independent. A gas mixture consisting of air, water and toluene vapors flows through the reactor under constant volume velocity and concentrations of all present substances; (b) the catalyst is deposited on the inner wall of the outer tube in a very thin layer and intraphase diffusion in the reaction path is negligible. With these main assumptions several model types can be derived, based on the physical picture, especially as regards hydrodynamics of the gas phase inside the reactor and the mode of toluene transfer from the gas phase to the catalytic surface. In this study we have derived three different reactor models.

3.6.2. Model I

The first model used in this modelling study was the heterogeneous one-dimensional (1D) model, based on the following additional assumptions [32]: (a) steady-state and isothermal conditions; (b) uniform pressure drop along the reactor; (c) ideal flow conditions through the reactor; (d) heterogeneous reaction on the catalyst surface deposited on the reactor's inner wall; (e) mass transfer occurring through the gas boundary layer near the catalyst surface; (f) intraphase (pore) diffusion neglected due to a very thin catalytic layer; (g) deactivation of the catalyst neglected because of the rapidly achieved stationary conversion of toluene and frequent changing catalyst layer. Considering the aforementioned facts, mass balances in the solid-phase (Eq. (7)) and in the gas phase (Eq. (8)) constitute the below model:

$$r_A = f(C_{A,s}) = k_g a(C_{A,g} - C_{A,s}) \tag{7}$$

$$u\frac{dC_A}{dz} = k_g a(C_{A,g} - C_{A,s}) \tag{8}$$

The initial conditions are

$$\text{at } z = 0 \quad C_{A,s} = C_{A,0} \text{ and } C_{A,g} = C_{A,0} \tag{9}$$

Interphase mass transfer coefficient, k_g, can be calculated taking into consideration the well-known empirical correlations [33]:

$$k_g = \frac{Sh\, D_A}{2R(1-\kappa)} \tag{10}$$

There are different literature correlations for calculation of Sherwood number, which usually have the following form:

$$Sh = f\left(Re, Sc, \frac{R}{L}\right) \tag{11}$$

This paper uses the correlation given by the expression [32]:

$$Sh = 0.705\left[Re\,\frac{R}{L}\right]^{0.43} Sc^{0.56} \tag{12}$$

3.6.3. Model II

A more realistic picture is obtained with concentration gradients across the reactor tube (gas phase) radius due to mass transfer by diffusion. This is a much better approximation then the previous ones because a sudden drop in the concentration at the boundary of a gas film and at equal toluene concentrations across the rest of the reactor's tube radius is unrealistic. Depending on the type of flow, two basic models can be derived. In the first model (Model II), only plug flow is considered in the axial direction and molecular diffusion transfer in the radial direction. This two-dimensional (2D) heterogeneous model differs from the 1D model only in that imaginary boundary layer is broadened over the whole space between the reactor's two concentric tubes and in that mass transfer in this region is only due to molecular diffusion. Model II consists of mass balance both in the gas phase (Eq. (13)) and in the solid phase (Eq. (14)):

$$u\frac{\partial C_A}{\partial z} + D_A\left(\frac{\partial^2 C_A}{\partial r^2} + \frac{1}{r}\frac{\partial C_A}{\partial r}\right) = 0 \tag{13}$$

$$r_A = -D_A\frac{\partial C_A}{\partial r} \tag{14}$$

Boundary conditions are: at catalyst surface, $r = R$, Eq. (14) is valid and at $r = 0$ (surface of the inner tube):

$$\frac{\partial C_A}{\partial r} = 0 \tag{15}$$

3.6.4. Model III

Under the assumed laminar flow through the reactor, radial dependence of velocity, $u(r)$, must be considered (Eq. (16)):

$$u(r) = 2u_m\left[1 - \left(\frac{r}{R}\right)^2\right] \tag{16}$$

where

$$u_m = \frac{v_0}{A_R} \tag{17}$$

Here $u(r)$ substitutes mean velocity in Eq. (13) and this is the only difference from the Model II.

3.7. Numerical solution

Mass balances for 1D model (Eqs. (7)–(9)) consist of the algebraic and 1st order ordinary differential equation, and they can be solved numerically by common methods. Eqs. (13)–(15) are partial differential equations and they can be solved by the appropriate numerical methods. The method of lines was applied in this study. The interphase mass transfer constant, k_g, in the 1D model is calculated using Eq. (10), while the value of the molecular diffusion coefficient of toluene in air, D_A for 2D models is taken from the literature ($0.0804\ cm^2\ s^{-1}$) [33]. Kinetic constant of the reaction rate, k_A, is regarded as the adjustable reactor parameter for all models. In some cases rate constant, k, and the adsorption coefficient, K_a, are regarded as the adjustable reactor parameters. Parameter estimation is performed using a modified differential method of data analysis and the Nelder–Mead method of non-linear optimisation.

Comparison of values obtained by Model I using the first-order kinetic model (Eq. (6)) and the LH mechanistic kinetic model (Eq. (5)) is shown in Fig. 4a. The estimated values of the rate constants (k_A) obtained using the pseudo-first order reaction rate are given in Table 1, while the estimated values of the rate constants (k) and the adsorption coefficient (K_a) obtained using LH mechanistic model are found to be: $0.5\ g\ dm^{-3}\ min^{-1}$ and $0.22\ dm^3\ g^{-1}$ at inlet toluene concentration of $3.1 \times 10^{-3}\ g\ dm^{-3}$ and $1.72\ g\ dm^{-3}\ min^{-1}$ and $0.23\ dm^3\ g^{-1}$ at inlet toluene concentration of $6.3 \times 10^{-3}\ g\ dm^{-3}$. As can be seen, satisfactory degree of correlation was established by both kinetic models. In addition, at lower inlet concentration of toluene almost the same theoretical predictions are obtained using both kinetic models. The agreement between the calculated and experimental results supports the

Table 1
Estimated rate constants, k_A and mean square deviations for different inlet toluene concentrations

$C_{A0} \times 10^3$ (g dm^{-3})	Model I		Model II		Model III	
	k_A/min^{-1}	SD $\times 10^2$	k_A (min^{-1})	SD $\times 10^2$	k_A (min^{-1})	SD $\times 10^2$
0.962	6.531	3.156	2.016	2.138	3.056	1.892
1.552	1.867	2.550	1.235	2.273	1.753	2.261
3.137	0.455	2.647	0.469	1.986	0.694	1.923
4.056	0.341	1.254	0.359	1.809	0.523	1.853
6.303	0.139	1.217	0.165	1.198	0.237	1.181
8.173	0.264	1.568	0.312	0.941	0.436	0.900

overall ability of the proposed models to describe kinetics of reaction.

Generally, both reactor models (1D and 2D) provide good agreement between the experimental data and theoretical predictions (Fig. 4b). However, taking into account the root of mean square deviation as a correlation criterion, better estimation results are obtained with 2D models. This fact supports the assumption of a more realistic hydrodynamic regime inside the annulus obtained with Models II and III. The difference between the results of Model II and Model III is very small, especially at low flow rates where laminar profiles in the fluid phase are not pronounced yet. The results reveal that the reaction rate constants, k_A, are decreased with the increased inlet toluene concentrations. Similar finding is reported in the literature [9,34]. The explanation may be competitive adsorption of the reaction by-products and the initial reactant at the active sites. If the number of active sites on TiO_2 surface is assumed constant, the increased inlet toluene concentration also increases competition between toluene and by-products (benzaldehyde and benzoic acid). This leads to decrease in the rate of toluene decomposition, confirmed by decreased estimated values of the reaction rate constants (Table 1). At the relatively high inlet toluene concentrations the rate of photocatalytic oxidation of toluene becomes almost independent of the total flow rate. This fact also confirms previous assumption and can be used for testing Langmuir isotherm. In Fig. 5, the profiles of normalized toluene fractions versus annulus diameter are presented at appropriate distances along the reactor length. Flat profile of toluene concentration occurs across the annulus diameter and is followed by a sharp fall in the region near the catalyst surface, especially at the entry to the reactor. These results indicate that the interphase mass transfer by molecular diffusion limits the reaction global rate and that the surface reaction rate is faster then mass transfer rate in the gas phase.

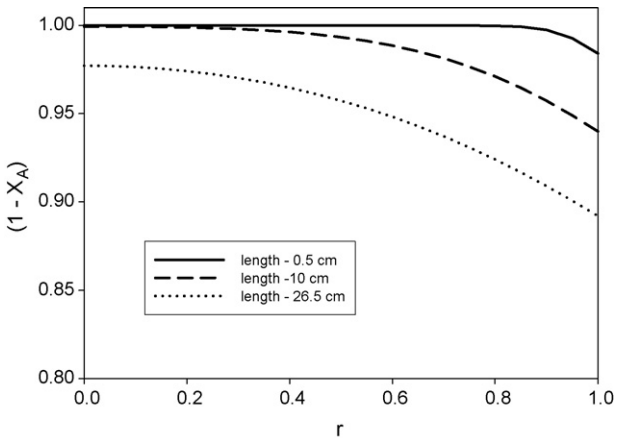

Fig. 5. Normalized toluene fractions versus dimensionless radius at the appropriate positions along the reactor length (reaction conditions: inlet toluene concentration = 0.96 $\times 10^{-3}$ g dm^{-3}, volume flow rate = 24.18 dm^3 h^{-1}; Model III).

4. Conclusions

This study dealt with photocatalytic oxidation of toluene in the gas phase in the annular fixed bed photocatalytic reactor. Several mathematical models of the PCO reactor (1D model and 2D models based on ideal flow and laminar flow conditions) were developed to understand complex reaction pathways and the reactor's limitation. The proposed models were verified by comparing computer simulation data with the experimental laboratory results. It is known that the 2D heterogeneous models are fairly complex, but they are superior in that toluene diffusion coefficient in the gas mixture, comprising mainly air, as the important reactor parameter is easily calculated. However, accuracy of empirical calculation of k_g included in the 1D heterogeneous model was much lower. The 2D heterogeneous model, based on the assumed laminar flow through the reactor, was found to be the best approximation of the physical nature of the photocatalytic annular reactor. Simulation result showed that the limiting step in the overall reaction system was the interphase mass transfer.

Acknowledgement

The authors highly appreciate financial support that the Ministry of Science, Education and Sport of Republic of Croatia has given for this study.

References

[1] H.D. Lasa, B. Serrano, M. Salaices, Photocatalytic Reaction Engineering, Springer, London, 2005, p. 17.
[2] A. Fujishima, K. Honda, Nature 238 (1972) 37.
[3] J. Zhao, X. Yang, Build. Environ. 38 (2003) 645.
[4] G.B. Raupp, A. Alexiadis, M.M. Hossain, R. Changrani, Catal. Today 69 (2001) 41.
[5] A. Mills, S.-K. Lee, J. Photochem. Photobiol. A: Chem. 152 (2002) 233.
[6] R.M. Alberici, W.F. Jardim, Appl. Catal. B: Environ. 14 (1997) 55.
[7] J.F. Hamilton, P.J. Webb, A.C. Lewis, M.R. Montserrat, Atmos. Environ. 39 (2005) 7263.
[8] S. Yamazaki, S. Tanaka, H. Tsukamoto, J. Photochem, Photobiol. A: Chem. 121 (1999) 55.
[9] A. Bouzaza, C. Vallet, A. Laplanche, J. Photochem, Photobiol. A: Chem. 177 (2006) 212.
[10] C. Xie, Z. Xu, Q. Yang, N. Li, D. Zhao, D. Wang, Y. Du, J. Mol. Catal. A: Chem. 217 (2004) 193.
[11] S.B. Kim, H.T. Hwang, S.C. Hong, Chemosphere 48 (2002) 437.
[12] F. Benoit-Marquié, U. Wilkenhöner, V. Simon, A.M. Braun, E. Oliveros, M.-T. Maurette, J. Photochem, Photobiol. A: Chem. 132 (2000) 225.
[13] J.-F. Wu, C.-H. Hung, C.-S. Yuan, J. Photochem, Photobiol. A: Chem. 170 (2005) 299.
[14] H. Ge, G. Chen, Q. Yuan, H. Li, Catal. Today 110 (2005) 171.
[15] N. Keller, E. Barraud, F. Bosc, D. Edwards, V. Keller, Appl. Catal. B: Environ. 70 (2007) 423.
[16] E. Obuchi, T. Sakamoto, K. Nakano, Chem. Eng. Sci. 54 (1999) 1525.
[17] V. Keller, P. Bernhardt, F. Garin, J. Catal. 215 (2003) 129.
[18] C.-P. Chang, J.-N. Chen, M.-C. Lu, H.-Y. Yang, Chemosphere 58 (2005) 1071.
[19] G.M. zuo, Z.-X. Cheng, H. Chen, G.-W. Li, T. Miao, J. Hazard. Mater. B 128 (2006) 158.
[20] C.S. Zalazar, C.A. Martin, A.E. Cassano, Chem. Eng. Sci. 60 (2005) 4311.
[21] D.W. Clarke, J.C. Joseph, J.P. Ferris, Icarus 147 (2000) 282.
[22] R. Mendez-Roman, N. Cardona-Martinez, Catal. Today 40 (1998) 353.
[23] M. Kang, S.-J. Choung, J.Y. Park, Catal. Today 87 (2003) 87.
[24] T.H. Lim, S.D. Kim, Chem. Eng. Proc. 44 (2005) 327.
[25] C. Nicolella, M. Rovatti, Chem. Eng. J. 69 (1998) 119.

[26] N.J. Peill, L. Bourne, M.R. Hoffmann, J. Photochem, Photobiol. A: Chem. 108 (1997) 221.
[27] S. Romero-Vargas Castrillón, H. Ibrahim, H.D. Lasa, Chem. Eng. Sci. 61 (2006) 3343.
[28] M.R. Hoffman, S.T. Martin, W. Choi, D.W. Bahnemann, Chem. Rev. 95 (1995) 69.
[29] L. Cao, Z. Gao, S.L. Suib, T.N. Obee, S.O. Hay, J.D. Freihauty, J. Catal. (2000) 253.
[30] V. Tomašić, Z. Gomzi, Chem. Eng. Proc. 43 (2004) 765.
[31] K. Demeestere, A.D. Visscher, J. Dewulf, M.V. Leeuwen, H.V. Langenhove, Appl. Catal. B: Environ. 54 (2004) 261.
[32] J. Votruba, J. Sinkule, V. Hlavaček, J. Skrivanek, Chem. Eng. Sci. 30 (1975) 117.
[33] U.S.E.p. agency, http://www.epa.gov/athens/learn2model/parttwo/onsite/estdiffusion.htm, 2007.
[34] Y. Ku, C.-M. Ma, Y.-S. Shen, Appl. Catal. B: Environ. 34 (2001) 181.